Inhibitory interneurons in a cortical column form hot zones of inhibition in layers 2 and 5A

Hanno S. Meyer[1], Daniel Schwarz, Verena C. Wimmer[2], Arno C. Schmitt[3], Jason N. D. Kerr[3], Bert Sakmann[1,4,5], and Moritz Helmstaedter[5]

Max Planck Institute for Medical Research, D-69120 Heidelberg, Germany

Contributed by Bert Sakmann, August 24, 2011 (sent for review April 21, 2011)

Although physiological data on microcircuits involving a few inhibitory neurons in the mammalian cerebral cortex are available, data on the quantitative relation between inhibition and excitation in cortical circuits involving thousands of neurons are largely missing. Because the distribution of neurons is very inhomogeneous in the cerebral cortex, it is critical to map all neurons in a given volume rather than to rely on sparse sampling methods. Here, we report the comprehensive mapping of interneurons (INs) in cortical columns of rat somatosensory cortex, immunolabeled for neuron-specific nuclear protein and glutamate decarboxylase. We found that a column contains ~2,200 INs (11.5% of ~19,000 neurons), almost a factor of 2 less than previously estimated. The density of GABAergic neurons was inhomogeneous between layers, with peaks in the upper third of L2/3 and in L5A. IN density therefore defines a distinct layer 2 in the sensory neocortex. In addition, immunohistochemical markers of IN subtypes were layer-specific. The "hot zones" of inhibition in L2 and L5A match the reported low stimulus-evoked spiking rates of excitatory neurons in these layers, suggesting that these inhibitory hot zones substantially suppress activity in the neocortex.

barrel cortex | parvalbumin | somatostatin | calretinin

For a quantitative understanding of the interaction between excitatory and inhibitory synaptic transmission in the neocortex, it is crucial to obtain data on the absolute numbers and the relative distribution of excitatory and inhibitory (mostly GABAergic) neurons [interneurons (INs)] in a cortical column. Only on the basis of such prevalence numbers is it possible to interpret data on single-cell physiology (1–8) and synaptic connections of pairs of neurons (9–12) at the circuit level. The distribution of cortical neurons and INs has therefore been the objective of several studies over the past decades (13–15). Statistical sampling methods were used because mapping tens of thousands of neurons was not feasible. Although the nominal error bounds of such methods are in the range of 10–20%, the reported absolute numbers differed strongly among studies, especially for sparse neuron populations, such as INs and their subtypes. The ratio of INs reported for the somatosensory cortex varied between 15% and 25%, thus by almost a factor of 2 (13, 16, 17). Data on possible differences in IN density between layers in a cortical column were contradictory (13, 15, 16, 18, 19).

To resolve these substantial discrepancies, we undertook the complete mapping of INs in entire cortical columns using the cytoarchitectonic barrels in L4 as a reference frame for the thalamocortical innervation volume (20) in postnatal day (P) 25–36 rat vibrissal cortex. Our data show that the overall prevalence of inhibitory neurons was previously overestimated by almost a factor of 2. We find a unique substructure of the distribution of INs in a cortical column that can explain the layer-specific differences in the excitability in neocortex. The distribution of INs defines layer 2 as a distinct neocortical layer.

Results

Delineation of Cortical Columns. For the measurement of IN distribution with reference to cortical columns, it was critical to define the borders of columns precisely for each of the neuron count datasets. We used the outlines of barrels in L4 of rat somatosensory cortex to define the lateral column borders (Fig. 1*A*). We had found previously that the overall epifluorescence of tissue stained against glutamate decarboxylase 67 (GAD67) showed barrel-related patches in L4 (corresponding to a high density of GAD67-positive boutons) and that these were aligned with the patches of thalamic afferents originating from the ventral posterior medial nucleus (21) (Fig. S1*A*). The column and layer borders derived from cytochrome C oxidase (CO)- and GAD67-stained slices agreed (average distance between corresponding column and layer borders: 14 ± 8 μm, Fig. 1*A*). For the following analyses, we used the column and layer borders derived from GAD67-stained slices.

Labeling of Neurons and INs. To identify somata of neurons and putative GABAergic INs, we double-immunolabeled 50-μm-thick slices against GAD67 and neuron-specific nuclear protein (NeuN). Fig. 1*B* shows fluorescence images obtained from the same optical section through L2/3 of a D2 column. Neurons were identified by NeuN staining, showing strong fluorescence in the soma and proximal dendrites (arrows in Fig. 1*B*, *Left*). Neurons were either GAD67-positive (filled arrow in Fig. 1*B*) or GAD67-negative (open arrow in Fig. 1 *B* and *C*). GAD67-positive neurons showed strong fluorescence in the somatic cytosol, whereas the nuclei remained unstained (filled arrow in Fig. 1*B*). GAD67-negative somata were delineated by surrounding GAD67-positive puncta, most likely representing GAD67-positive boutons (cf. 22) (open arrow in Fig. 1*B*, *Center*).

GAD, the synthesizing enzyme of GABA, is thought to be a reliable marker of GABAergic neurons (e.g., 22–24). We correlated GAD67 antigenicity with staining against GABA by immunolabeling 50-μm-thick slices for NeuN, GABA, and GAD67 (Fig. 1*C*). NeuN-positive neurons (Fig. 1*C*, arrows) were either clearly GABA-negative (Fig. 1*C*, *Upper Left*, open arrow), clearly GABA-positive (Fig. 1*C*, filled arrow), or neither clearly negative nor clearly positive (Fig. 1*C*, dashed arrow). All clearly GABA-positive neurons were positive for GAD67 (71 of 71). Eight of 96 GAD67-positive neurons were clearly GABA-negative. We conclude that GAD67 immunolabeling was highly sensitive to GABA-positive

Author contributions: H.S.M., B.S., and M.H. designed research; H.S.M., A.C.S., and J.N.D.K. performed research; V.C.W. contributed new reagents/analytic tools; H.S.M., D.S., and M.H. analyzed data; and H.S.M. and M.H. wrote the paper.

The authors declare no conflict of interest.

Freely available online through the PNAS open access option.

[1]Present address: Department of Digital Neuroanatomy, Max Planck Florida Institute, Jupiter, FL 33458.

[2]Present address: Florey Neuroscience Institutes, University of Melbourne, Parkville 3010, Victoria, Australia.

[3]Present address: Network Imaging Group, Max Planck Institute for Biological Cybernetics, 72076 Tubingen, Germany.

[4]Present address: Research Group Cortical Column in Silico, Max Planck Institute for Neurobiology, D-82152 Martinsried, Germany.

[5]To whom correspondence may be addressed. E-mail: bert.sakmann@maxplanckflorida.org or moritz.helmstaedter@mpimf-heidelberg.mpg.de.

This article contains supporting information online at www.pnas.org/lookup/suppl/doi:10.1073/pnas.1113648108/-/DCSupplemental.

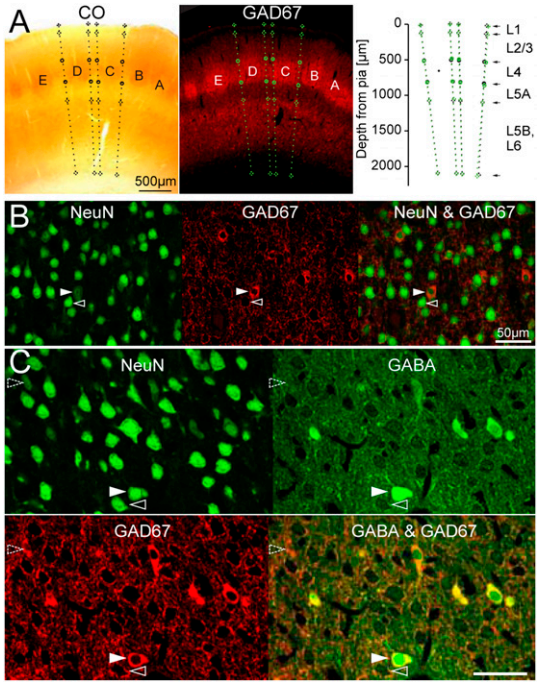

Fig. 1. Identification of columns, neurons, and INs. (*A*) (*Left*) Bright-field image of a CO-stained semicoronal barrel cortex slice (100-µm thickness, right hemisphere, P27 rat). Note barrels as dark patches in L4. Borders of cortical columns were extrapolated from the lateral barrel borders (dashed lines). (*Center*) Epifluorescence image of the subsequent slice (50 µm), immunolabeled for GAD67. Note clearly visible barrels (Fig. S1). (*Right*) Column and layer outlines from the CO staining (black) and GAD67 staining (green). (*B*) Fluorescence images of a slice immunolabeled for NeuN and GAD67 and an overlay. A GABAergic IN (filled arrow) and GAD67-negative (excitatory) neuron (open arrow) are indicated. (*C*) Fluorescence images of a slice immunolabeled for GABA in addition to NeuN and GAD67. The filled arrow shows a GABA- and GAD67-positive neuron; the open arrow shows a GABA- and GAD67-negative neuron; and the dashed arrow shows a GAD67-positive and GABA-ambiguous neuron. All images in *B* and *C* show one confocal imaging plane. (Scale bar: 50 µm.)

neurons and that the following analyses using GAD67 antigenicity yield an upper estimate of GABA-positive neuron densities. In the following, we use the term "interneuron" for GAD67-positive GABAergic neurons.

Distribution of the Somata of INs in Putative Cortical Columns. We first analyzed the IN distribution in five slices cut at a thickness of 50 µm through the center of the D2 column. Five slices from five hemispheres of four animals (P25–P36, both sexes) were analyzed. All the slices contained the center of D2 ($n = 5$) and either C2 ($n = 3$) or E2 ($n = 2$). Markers were manually placed in somata of neurons and INs [details, especially the correction for double-counting between slices, are discussed in the article by Meyer et al. (21) and *SI Materials and Methods*]. Fig. 2 *A* and *B* shows the neuron and IN markers from one of the slices (9,911 neuron somata in Fig. 2*A* and 1,334 IN somata in Fig. 2*B*). For quantification, we computed 2D neuron and IN density maps in the plane of the slice (Fig. S2). Finally, to calculate average density maps, the soma markers from the five slices were registered to a standard D2 column 2 mm in height aligned at the L4 barrel center, with the vertical column axis approximately perpendicular to the pial surface. Density maps were smoothed and interpolated (*SI Materials and Methods* and Fig. S3). Fig. 2 *C* and *D* shows the resulting average smoothed interpolated density maps of excitatory neuron (Fig. 2*C*) and IN (Fig. 2*D*) somata centered on the D2 barrel. The projection of these maps onto the vertical column axis is shown in Fig. 2 *E* and *F*.

The density of IN somata was highest at a depth of 180–210 µm in upper L2/3 (18,400 per mm^3, Fig. 2 *D* and *F*) and at a depth of 800–1,100 µm in infragranular layers (14,000 per mm^3). IN density dropped by a factor of 1.9 from upper L2/3 to lower L2/3 (17,400 vs. 9,000 per mm^3, Fig. 2 *D* and *F* and Table 1). The IN density profile thus suggested a distinction of L2 and L3 that was not observed previously based on either the excitatory neuron density [Fig. 2 *C* vs. *D* and Fig. 2 *E* (black line) vs. *F*] or bright-field images of CO-stained slices (Fig. 1). The depth dependence of the soma density as seen in the *Z*-profiles (Fig. 2 *E* and *F*) allowed a quantitative delineation of the L2-to-L3 border. We determined the steep drop in IN density within L2/3 to be at 240 µm from the pia (i.e., at 37% of the layer 2/3 height; Fig. 2*F*). This thus defines a division of "L2/3" into layer 2 and layer 3 with a relative thickness of approximately one-third (L2) vs. two-thirds (L3).

In the tangential plane, lateral column borders could be delineated at the level of layer 4 based on neuron soma density (Fig. 2 *A* and *C*). The delineation of lateral column borders by NeuN-positive soma density was not observed in supra- or infragranular layers (21) (Fig. 2*C*). The distribution of IN somata, however, showed an outline of the lateral border between the D2 column and its neighboring columns at a depth of 200–300 µm in lower L2 and upper L3 (Fig. 2*D*, arc-like shaped band of high soma density; Fig. 3; and as discussed below). Thus, the distribution of INs may suggest a cytoarchitectonic columnar pattern even in supragranular layers.

Neuron and IN Distribution in Complete Cortical Columns. We next counted INs in three complete cortical columns (C2, D2, and D3) to obtain a reliable measurement of the absolute number of INs in

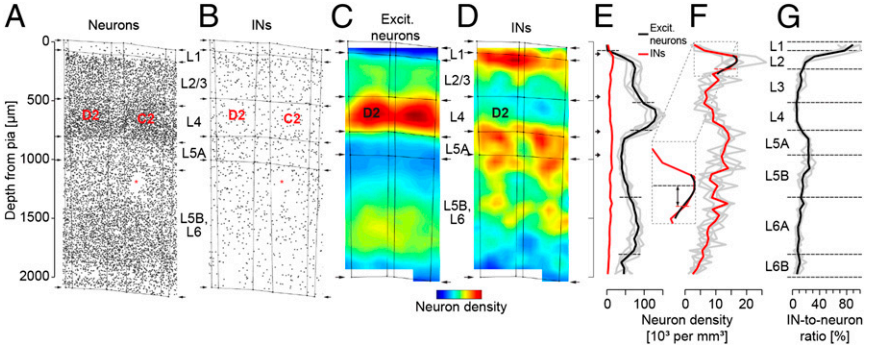

Fig. 2. Distribution of excitatory neurons and INs in cortical columns. (*A*) Distribution of NeuN-positive somata in one semicoronal slice (thickness of 50 µm, 9,801 manually placed markers). Dashed lines show column and layer borders determined by GAD67 staining (Fig. 1*A*). Note the barrel-aligned patches of high neuron density in L4 (Fig. S2*A*). (*B*) Distribution of GAD67-positive somata in the same slice (1,209 markers; Fig. S2*B*). Maps of average excitatory neuron density (*C*) and GAD67-positive IN density (*D*) from five slices centered at the D2 column, aligned to the D2 barrel center (*Materials and Methods* and Fig. S3). Note the two IN "hot zones" in L2 and upper L5 defined by high IN density, whereas IN density in L3, L4, and lower L6 is low. (Color scale bar range: *C*, 0–140,000 per mm^3; *D*, 0–18,500 per mm^3.) (*E*) IN density distribution along the D2 vertical column axis (red), mean excitatory neuron density (black), and individual density profiles from the five slices (gray). Layer borders were determined by differences in excitatory neuron density (dashed horizontal lines). (*F*) Mean IN density profile (as in *E*), with a sharp peak in supragranular layers defining a cytoarchitectonic layer 2 (*Inset*). (*G*) IN-to-neuron ratio along the vertical column axis (D2 column). Red markers in *A* and *B* indicate a blood vessel.

Table 1. Number and density of INs in the layers of a cortical column

	Entire columns (C2, D2, D3)				Slices (3 × C2, 3 × D2)	
Layer	No. excitatory neurons	No. INs	IN density, 10^3 per mm^3*	IN-to-neuron ratio (%)	IN density, 10^3 per mm^3*	IN-to-neuron ratio (%)
1	10 ± 7	53 ± 6	5.5 ± 2.2	84.3 ± 9.5	4.6 ± 1.9	96.8 ± 5.1
2	1,701 ± 484	338 ± 40	14.5 ± 0.7	17 ± 2.4	14.5 ± 3.2	20.8 ± 2.7
3	3,398 ± 807	338 ± 109	9.1 ± 1.5	9 ± 1.1	8.9 ± 2.1	9.5 ± 1.7
4	4,089 ± 425	358 ± 15	10 ± 1.1	8.1 ± 0.5	9.2 ± 1.4	6.4 ± 0.7
5A	1,394 ± 247	343 ± 65	10.9 ± 3	19.9 ± 4.1	13.4 ± 1.8	20.5 ± 3
5B	1,873 ± 53	362 ± 62	9.7 ± 1.9	16.2 ± 2.1	11.4 ± 2.2	18.3 ± 2.8
6A	3,449 ± 165	337 ± 31	8.2 ± 0.8	8.9 ± 0.9	8.7 ± 0.5	9.7 ± 0.8
6B	976 ± 155	90 ± 17	3.5 ± 0.4	8.4 ± 0.6	4.8 ± 1.2	8.7 ± 2.7
L1–6B	16,889 ± 423	2,220 ± 198	9.2 ± 0.9	11.6 ± 1	9.8 ± 0.8	12.1 ± 0.6

All numbers are mean ± SD.
*The volume density is sensitive to tissue shrinkage. Calibration in the living brain (Fig. S7) yielded a shrinkage estimate of up to 20% per spatial dimension.

a cortical column (because these results were not affected by tissue shrinkage, as discussed below; Table 1). These data also allowed us to investigate the IN distribution in the tangential plane further. The number and distribution of all neurons in these three columns have been reported previously (21). Fig. 3 *A* and *B* shows the neuron and IN somata detected in consecutive tangential slices at a thickness of 50 μm containing D2 and C2 in the right hemisphere of a P27 animal. The high IN density in L2 and L5A is visible (Fig. 3*B*). Together with a mapping of all INs in the D3 column (Fig. 3*D*), these data permitted the analysis of IN distributions in the tangential plane (parallel to the surface of the cortex). We determined the vertical column axes for each of the three columns (Fig. 3*D*) and then rotated the three datasets to the common axis and aligned them to the barrel center in the tangential plane (Fig. 3*E*). We then computed IN density maps in the tangential plane (Fig. 3*F*) at increasing depths from the pia. The arc-like shaped band of high IN soma density seen in the supragranular layers in the average semicoronal slice of the center of the D2 column (compare with Fig. 2*D*) was indeed indicative of a circular distribution of high IN soma density in lower L2 and upper L3 (Fig. 3*F*, *Upper Middle*). Note, however, that this putative columnar distribution appeared at a depth of 50–150 μm from the pia in the whole-column analysis (Fig. 3*F*), whereas it appeared at a depth of approximately 200–300 μm in the semicoronal slice data (Fig. 2*D*) because the latter were normalized to a standard column with a height of 2 mm.

Molecular Markers of INs in a Cortical Column. Parvalbumin (PV), somatostatin (SOM), and calretinin (CR) are widely used as molecular markers of INs (e.g., 25–28). We triple-immunolabeled slices of D2 and C2 for NeuN and GAD67 as well as for either PV, SOM, or CR. Virtually all marker-positive neurons were also positive for GAD67 (97.4% for SOM, 97.8% for PV, and 98.1% for CR), supporting the assumption that GAD67 immunohistochemistry (IHC) labels almost all inhibitory INs. Density maps showing the distributions of immunoreactive somata are shown in Fig. 4 (also in Figs. S4 and S5). We found that PV-positive INs were most abundant in lower L4 and infragranular layers (Fig. 4 *A* and *D*); SOM-positive INs were most abundant in L3, L5A, and L6A (Fig. 4 *B* and *D*); and CR-positive INs showed highest densities in L2 and L5B (Fig. 4 *C* and *D*). In all cortical layers, with the exception of L6B, the density of PV-positive INs was higher than the density of SOM- or CR-positive INs (Fig. 4*D*). On average, PV-positive INs, SOM-positive INs, and CR-positive INs ac-

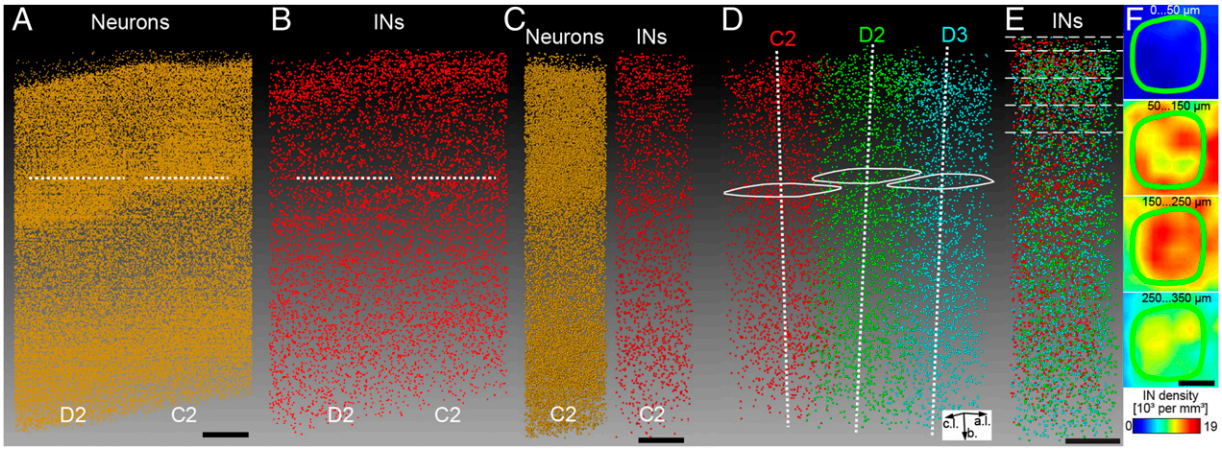

Fig. 3. IN distribution in three complete cortical columns. Projection in a semicoronal plane of 66,422 NeuN-positive (*A*) and 7,389 GAD67-positive (*B*) soma markers in a region comprising the entire D2 and C2 columns. Dashed lines represent barrel outlines in the tangential plane. Note the high density of INs in L2 and L5A. (*C*) Neuron distribution (*Left*) and IN distribution (*Right*) in the C2 column, rotated to the vertical column axis. (*D*) IN distribution in three complete columns (C2, D2, and D3: red, green, and blue, respectively). Dashed lines represent vertical column axes, and white lines represent barrel outlines. a.l., anterior-lateral; b., basal; c.l., caudal-lateral. (*E*) Overlay of the 6,686 INs counted in three columns (*D*), aligned to the column axis and the pial surface and centered (in the tangential plane) to the barrel center. (*F*) Distribution of INs in the tangential plane. Density maps at varying depths from the pia (dashed white lines in *E*). Note the ring-like distribution of INs at 50–150 μm from the pia (corresponding to the "arcs" seen in the semicoronal plane; Fig. 2*D*). (Scale bars: 200 μm.)

counted for 76% of GAD67-positive INs (Fig. 4*E*). Note, however, that in L2 and lower L6, the total of the three markers did not account for more than 50% of all INs (as little as ∼40% in L2), leaving at least half of the IN population unaccounted for. In L1, where all neurons are INs (Fig. 2*G*), virtually no marker-positive neurons were found.

Absolute Number of INs in a Cortical Column. We finally calculated the absolute number of INs in the layers of an average barrel column (Table 1; for INs in the white matter, see Fig. S6). When based on extrapolations from volume densities and column geometry, such absolute numbers are very sensitive to tissue shrinkage (attributable to fixative-mediated dehydration) and the precise definition of column borders. Using two-photon laser scanning microscopy, we measured the density of neurons in upper layer 2 in the D2 barrel column in vivo, yielding a lower bound estimate of the volume density of 53,000 neurons per mm^3 (29) (Fig. S7). Comparing this with the average L2 neuron density in fixed tissue (Table 1), we found that tissue volume shrinkage is significant: up to 20% per spatial dimension. We therefore counted all INs in completely reconstructed columns (Fig. 3) to obtain absolute numbers of INs per layer in a cortical column that were unaffected by shrinkage, as we reported previously for absolute numbers of all neurons in a cortical column (21). Comparing the density measurements obtained from semicoronal slices of the D2 column center (Fig. 2) with data from entire column counts (Fig. 3) yielded no significant differences in any of the layers (Table 1). Both measurements agreed on the estimated IN ratio (11.6% vs. 12.1%, respectively; Table 1).

In summary, we find that a cortical column contains ∼2,200 INs. All layers comprise ∼300–400 INs, with the exception of layers 1 and 6B (50 and 90 INs, respectively). The fraction of neurons that is GABAergic is, on average, 11–13%; it approaches 20% only in layers 2 and 5A.

Discussion

By counting IN distributions with reference to the geometrical landmarks of cortical columns, we found that (*i*) the fraction of INs is lower than previous estimates (∼11–12%, totaling ∼2,200 INs per cortical column); (*ii*) the distribution of INs is more inhomogeneous along the vertical column axis than previously reported ("hot zones" of IN density are located in upper L2/3 and in L5A); (*iii*) the density and fraction of GABAergic INs define a genuine cytoarchitectonic layer 2 in vibrissal cortex, with L2 comprising the upper one-third and L3 comprising the lower two-thirds of L2/3; and (*iv*) the IN distribution in the tangential plane indicates column borders in supragranular layers.

Fraction and Density of INs: Comparison with Previous Reports. Previous reports of the fraction of INs in rat somatosensory cortex yielded estimates between 15% (13) and 25% (16), thus differing by a factor of 1.7. Our data show that the fraction of INs is, in fact, lower (12%, Table 1). Notably, this low IN fraction was confirmed both by the whole-column counts (12.1% ± 0.6%, obtained from tangential slices; Fig. 3) and the center-column counts (11.6% ± 1%, obtained from coronal slices; Fig. 2).

Data on the inhomogeneity of IN density between cortical layers has been most controversial, even for the same species (rat) and cortical area (somatosensory cortex): Beaulieu (13) reported only moderate differences between layers; Ren et al. (16) reported strong differences, with the highest IN density in layer 4; Esclapez et al. (19) reported the highest densities for infragranular layers; and Chmielowska et al. (18) reported the highest densities for supragranular layers. Our data show that the IN volume densities are, in fact, highest in L2 and L5A and that they are almost 50% lower in L4 (Table 1). Moreover, the fraction of INs is lowest in L4 (only 8.1 ± 0.5%).

Methodological Considerations. Methodological differences (cf. 21) may explain the discrepancies from previous reports. Analysis of the number and distribution of less prevalent neuronal populations (e.g., INs, subtypes of INs) in small cortical volumes (e.g., single cortical columns, layers and sublayers of a single cortical column) requires the localization of a large number of neurons, preferably in the complete volume of interest, as was done in the present study. Previous studies, however, used Nissl staining and GABA IHC of very thin slices and random statistical sampling of only a few somata (disector method), which may have hampered these analyses, as indicated by their disagreeing results (13, 16). In the present study, using IHC of consecutive thick sections in combination with confocal microscopy, mosaic scanning, visualization software, and computer-aided data analysis, the actual counting of tens of thousands of neurons and differentiation of columns from the surrounding cortex were feasible (21, 30). The data presented here are from adolescent rats. It is unknown whether the IN distribution that we found is species-specific, which will be an important topic for future studies.

IN Density Defines a Genuine Layer 2 in Cortex. Historically, the basis of the laminar subdivision of isocortex is the Nissl preparation (31), mainly revealing differences in size, shape, and packing density of the pyramidal cells as a basis for the distinction of cortical layers (32–34). L2 has been described as the "corpuscular layer" and L3 as the "pyramidal layer" (33, 35, 36). Many attempts were made to identify specific anatomical features distinguishing L2 and L3 in specific cortical areas [e.g., higher density of stellate and small pyramidal cells in L2 vs. fewer stellate cells and a sparser

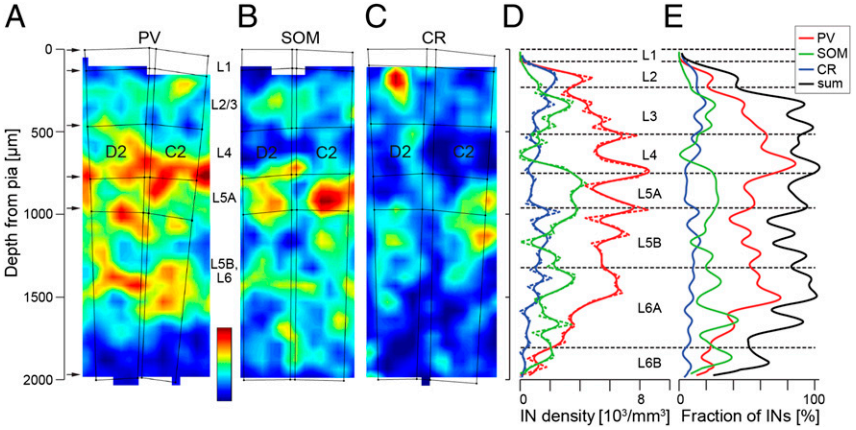

Fig. 4. Distribution of IN somata immunoreactive for PV, SOM, and CR. Average density maps of PV-positive (*A*), SOM-positive (*B*), and CR-positive (*C*) INs in slices from the D2 and C2 columns (compare with Fig. S4). (*D*) Distribution of the IHC IN types along the vertical column axis (D2 column; variability between individual slices is shown in Fig. S5). Note that PV-positive INs are most dense in lower L4; SOM-positive INs are most dense in L5A, L3 and upper L6; and CR-positive IN density has a peak in L2 and L5B. (*E*) Vertical profile of the fraction of IHC IN types (compared with all INs in the D2 column). Note that in all layers except for L6B, PV-positive INs are most abundant and the majority of INs are negative for all three tested markers (sum of ratios, black line) in L2, although IN density is highest (Fig. 2 *D*–*G*). Only in lower L3, L4, and upper L6A can the three IN markers account for all INs. (Color scale bar, neuron density range: *A*, 0–11,000 per mm^3; *B*, 0–6,000 per mm^3; *C*, 0–4,000 per mm^3.)

population of larger pyramidal cells in L3 of visual cortex (37–39), a density gradient from L2 to L3 of vertically projecting INs in an ^{3}H-GABA uptake study (40), or an indication of a density peak in L2 found in some samples taken from monkey cortex (41, cf. 13, 16–18)]. However, because of the lack of clearly distinguishing anatomical features under most experimental conditions, L2 and L3 were treated as one layer (L2/3) in most physiological studies (e.g., 8, 10, 11, 42–45). Recently, evidence for functional differences in electrical activity between L2 and L3 has accumulated from different cortical areas, such as somatosensory barrel cortex (2, 46, 47) and visual cortex (48). Here, we report data that provide a quantitative basis for a clear anatomical separation of L2 and L3 based on the distribution of the cell bodies of inhibitory neurons.

In a recent counting study in mouse vibrissal cortex, layers 2 and 3 were reported to have almost equal IN density (49). The precise geometrical alignment of the soma distribution may be critical for finding distribution patterns of sparse neuron populations, although species difference remains a possible explanation.

IN Distribution Within Columns. In the tangential plane, lateral borders of cortical columns could be delineated in neuron density maps within L4 and in IN density maps within L2 (Figs. 2 and 3). The column delineation based on IN density corresponded to an "arc-like" surround in the upper supragranular layers with an increased IN density in the septa within L2, and it could also be seen in the whole-column count experiments (Fig. 3*F*). The width between the high IN density "arcs" in L2 corresponded roughly to the barrel width (Fig. 2*D*), which would also indicate a cylindrical outline of a cortical column in supragranular layers. This finding can also be taken as supporting the assumption that cortical columns are relevant functional units in neocortex beyond the cortical input layer 4 (50–52) [a different view on cortical columns is presented elsewhere (53, 54)].

Molecular Markers PV, SOM, and CR. Several molecular markers have been used to label putatively distinct subgroups of INs (25, 26, 55, 56). Our data suggest that the coverage of the overall IN population by PV, SOM, and CR is, at most, ~75% (Fig. 4). This number represents an upper estimate, because we labeled for one marker at a time and coexpression of a second marker is likely to occur (55). Coverage was extremely low in L1, L2, lower L6A, and L6B. The PV-, SOM-, and CR-negative INs may be immunoreactive for ionotropic serotonin receptors, which have recently been shown to be expressed in virtually all SOM- and PV-negative INs in mouse neocortex (57).

Functional Interpretation. Juxtacellular recordings in vivo from excitatory neurons in all layers of cortical columns during stimulation of a rat's whiskers have shown that evoked action potential firing is extremely low in layers 2 and 5A (5). We argue that our finding of high IN soma densities in these layers provides evidence for an inhibitory origin of this suppression of activity. However, we have only quantified IN soma density, and to obtain correct quantitative predictions of inhibitory innervation density, the axonal distributions have to be taken into account (58). Although this remains an important issue for future studies, it can be noted that most INs have a very high perisomatic axon density, in addition to their specific projection patterns (59). This high perisomatic axon density predicts strong inhibitory effects in those layers that have a high density of IN somata.

Outlook. To build detailed mechanistic models of cortical function (50), single cells representative of distinct anatomically and functionally defined groups of excitatory and inhibitory neurons have to be placed throughout the layers of a cortical column at sufficient spatial precision and in the correct quantity. The data on the number of inhibitory neurons within the layers of a barrel column reported here, together with data on innervation probabilities and axonal projection patterns (10, 58, 59), will serve as a basis for reconstructing the inhibitory synaptic circuits within and between cortical columns.

Materials and Methods

Preparation. Experimental procedures were conducted in accordance with the German Animal Welfare Act. Wistar rats (aged 25–36 d) of both sexes were perfused transcardially, and brains were removed and fixed with paraformaldehyde (PFA) as described previously (21). For experiments that included GABA immunolabeling, animals were perfused with 1 mL/g body weight of 50 mM cacodylic acid and 1% Na-bisulfite (pH 6.2), followed by 0.5 mL/g body weight of 100 mM cacodylic acid, 1% Na-bisulfite, 4% (g/l) PFA, and 0.3% glutaraldehyde (postfixation for 2 h). Semicoronal slices of the posteromedial barrel subfield were cut at a thickness of 50 μm as described previously (21).

Histological Procedures. Slices were double-immunolabeled for the 67-kDa isoform of GAD67 and NeuN using monoclonal mouse primary antibodies and isotype-specific secondary anti-mouse IgG antibodies, as described previously (21). In some experiments, GAD67 and NeuN immunolabeling was combined with immunolabeling for PV, SOM, or CR; both the 65- and 67-kDa isoforms of GAD; or GABA. Primary antibodies (all from Chemicon) were used at the following concentrations: 1:800 mouse anti-GAD67 (IgG2a subtype), 1:500 mouse anti-NeuN (IgG1 subtype), 1:2,000 rabbit anti-PV, 1:4,000 rabbit anti-CR, 1:500 rabbit anti-GAD65/67, or 1:200 rat anti-SOM, treated with an Alexa 488 monoclonal antibody labeling kit (Invitrogen). For PV, CR, and GAD6567 experiments, the following secondary antibodies (all from Invitrogen) were used: 1:500 goat anti-mouse IgG2a Alexa 488, 1:500 goat anti-mouse IgG1 Alexa 350 or 647, or 1:100 goat anti-rabbit Alexa 555. For SOM experiments, secondary antibodies (both from Invitrogen) were 1:500 goat anti-mouse IgG2a Alexa 555 and 1:500 goat anti-mouse IgG1 Alexa 647. They were incubated at room temperature in phosphate buffer (PB) containing 1.5% normal goat serum (NGS) for 2–3 h. For GABA experiments, slices were permeabilized and blocked in 0.5% Triton X-100 (TX) (Sigma-Aldrich) in 50 mM Tris and 1% Na-bisulfite (pH 7.5) containing 4% (vol/vol) NGS for 1.5 h. Primary antibodies (1:800 mouse anti-GAD67, 1:500 mouse anti-NeuN, and 1:250 rabbit anti-GABA; Chemicon) were incubated at 4 °C in 50 mM Tris and 1% Na-bisulfite (pH 7.5) containing 1% NGS and 0.5% TX for 42 h. Secondary antibodies (1:500 goat anti-mouse IgG2a Alexa 488, 1:500 goat anti-mouse IgG1 Alexa 647, and 1:100 goat anti-rabbit Alexa 555) were incubated at room temperature in 50 mM Tris and 8.5 g/L NaCl (pH 7.5) containing 3% NGS and 0.3% TX for 2 h. Slices were mounted on slides, embedded with SlowFade Gold (Invitrogen), and enclosed with a coverslip.

In some experiments, selected slices were cut at a thickness of 100 μm and stained for CO (60).

Image Acquisition. Slices were imaged using a BX51 (Olympus) microscope at a magnification of 4× (N.A. of 0.10). Confocal microscopy using TCS SP2 and SP5 confocal laser scanning microscopes equipped with a 40× (N.A. of 1.25) oil immersion objective (Leica Microsystems) and mosaic scanning were conducted as described previously (21). Details are provided in *SI Materials and Methods*.

Manual Placement of Soma Markers and Delineation of Cortical Columns and Layers. 3D soma positions of NeuN-positive neurons were obtained as described previously (21). Briefly, markers were placed in the center of the somata. To correct for edge effects at the borders between slices, somata were only counted if more than half of the soma was imaged (as judged by the diameter change). We had previously found the systematic error attributable to these effects to be less than 5% (21). Somata of inhibitory INs were marked in the GABA and the GAD67 fluorescence channels accordingly, as were somata that were immunoreactive for molecular markers (PV, SOM, and CR).

The horizontal borders of columns, and layer borders, were determined based on GAD67 or CO staining, as described previously (21), with the exception of the L2-to-L3 border. Details are provided in *SI Materials and Methods*.

Soma Densities and Absolute Soma Counts. Five slices from five hemispheres of four animals were analyzed (P25: left hemisphere, D2 and C2; P26: right hemisphere, D2 and C2; P27: right hemisphere, D2 and C2; and P36: right and left hemisphere, D2 and E2). All the slices contained the center of D2 ($n = 5$) and either C2 ($n = 3$) or E2 ($n = 2$). Soma distributions were analyzed using custom-made software written in MATLAB (MathWorks), as discussed in *SI Materials and Methods*.

ACKNOWLEDGMENTS. We thank Dr. K. L. Briggman for discussions; M. Kaiser and H. Erdal for technical assistance; Dr. G. Giese for providing the confocal imaging facility; and Dr. K. Rohm, W. Kaiser, and K. Bauer for information technology support. We thank A. Ayache, Z. Aydin, R. Kolibas, S. Moughal, H. Peykarjou, B. Pickard, and G. Quispe for neuron counting.

1. Pouille F, Scanziani M (2001) Enforcement of temporal fidelity in pyramidal cells by somatic feed-forward inhibition. *Science* 293:1159–1163.
2. Brecht M, Roth A, Sakmann B (2003) Dynamic receptive fields of reconstructed pyramidal cells in layers 3 and 2 of rat somatosensory barrel cortex. *J Physiol* 553: 243–265.
3. Brecht M, Sakmann B (2002) Dynamic representation of whisker deflection by synaptic potentials in spiny stellate and pyramidal cells in the barrels and septa of layer 4 rat somatosensory cortex. *J Physiol* 543:49–70.
4. Manns ID, Sakmann B, Brecht M (2004) Sub- and suprathreshold receptive field properties of pyramidal neurones in layers 5A and 5B of rat somatosensory barrel cortex. *J Physiol* 556:601–622.
5. de Kock CP, Bruno RM, Spors H, Sakmann B (2007) Layer- and cell-type-specific suprathreshold stimulus representation in rat primary somatosensory cortex. *J Physiol* 581:139–154.
6. de Kock CP, Sakmann B (2008) High frequency action potential bursts (>or= 100 Hz) in L2/3 and L5B thick tufted neurons in anaesthetized and awake rat primary somatosensory cortex. *J Physiol* 586:3353–3364.
7. Gabernet L, Jadhav SP, Feldman DE, Carandini M, Scanziani M (2005) Somatosensory integration controlled by dynamic thalamocortical feed-forward inhibition. *Neuron* 48:315–327.
8. Kapfer C, Glickfeld LL, Atallah BV, Scanziani M (2007) Supralinear increase of recurrent inhibition during sparse activity in the somatosensory cortex. *Nat Neurosci* 10: 743–753.
9. Murayama M, et al. (2009) Dendritic encoding of sensory stimuli controlled by deep cortical interneurons. *Nature* 457:1137–1141.
10. Helmstaedter M, Staiger JF, Sakmann B, Feldmeyer D (2008) Efficient recruitment of layer 2/3 interneurons by layer 4 input in single columns of rat somatosensory cortex. *J Neurosci* 28:8273–8284.
11. Reyes A, et al. (1998) Target-cell-specific facilitation and depression in neocortical circuits. *Nat Neurosci* 1:279–285.
12. Holmgren C, Harkany T, Svennenfors B, Zilberter Y (2003) Pyramidal cell communication within local networks in layer 2/3 of rat neocortex. *J Physiol* 551:139–153.
13. Beaulieu C (1993) Numerical data on neocortical neurons in adult rat, with special reference to the GABA population. *Brain Res* 609:284–292.
14. Gabbott PL, Somogyi P (1986) Quantitative distribution of GABA-immunoreactive neurons in the visual cortex (area 17) of the cat. *Exp Brain Res* 61:323–331.
15. Fitzpatrick D, Lund JS, Schmechel DE, Towles AC (1987) Distribution of GABAergic neurons and axon terminals in the macaque striate cortex. *J Comp Neurol* 264:73–91.
16. Ren JQ, Aika Y, Heizmann CW, Kosaka T (1992) Quantitative analysis of neurons and glial cells in the rat somatosensory cortex, with special reference to GABAergic neurons and parvalbumin-containing neurons. *Exp Brain Res* 92:1–14.
17. Jones EG (1993) GABAergic neurons and their role in cortical plasticity in primates. *Cereb Cortex* 3:361–372.
18. Chmielowska J, Stewart MG, Bourne RC (1988) gamma-Aminobutyric acid (GABA) immunoreactivity in mouse and rat first somatosensory (SI) cortex: Description and comparison. *Brain Res* 439:155–168.
19. Esclapez M, Campistron G, Trottier S (1987) Immunocytochemical localization and morphology of GABA-containing neurons in the prefrontal and frontoparietal cortex of the rat. *Neurosci Lett* 77:131–136.
20. Wimmer VC, Bruno RM, de Kock CP, Kuner T, Sakmann B (2010) Dimensions of a projection column and architecture of VPM and POm axons in rat vibrissal cortex. *Cereb Cortex* 20:2265–2276.
21. Meyer HS, et al. (2010) Number and laminar distribution of neurons in a thalamocortical projection column of rat vibrissal cortex. *Cereb Cortex* 20:2277–2286.
22. Ribak CE, Vaughn JE, Saito K (1978) Immunocytochemical localization of glutamic acid decarboxylase in neuronal somata following colchicine inhibition of axonal transport. *Brain Res* 140:315–332.
23. Staiger JF, et al. (2002) Excitatory and inhibitory neurons express c-Fos in barrel-related columns after exploration of a novel environment. *Neuroscience* 109:687–699.
24. Ribak CE (1978) Aspinous and sparsely-spinous stellate neurons in the visual cortex of rats contain glutamic acid decarboxylase. *J Neurocytol* 7:461–478.
25. Kawaguchi Y, Kubota Y (1997) GABAergic cell subtypes and their synaptic connections in rat frontal cortex. *Cereb Cortex* 7:476–486.
26. Gonchar Y, Burkhalter A (1997) Three distinct families of GABAergic neurons in rat visual cortex. *Cereb Cortex* 7:347–358.
27. Cauli B, et al. (2000) Classification of fusiform neocortical interneurons based on unsupervised clustering. *Proc Natl Acad Sci USA* 97:6144–6149.
28. Cauli B, et al. (1997) Molecular and physiological diversity of cortical nonpyramidal cells. *J Neurosci* 17:3894–3906.
29. Kerr JN, et al. (2007) Spatial organization of neuronal population responses in layer 2/3 of rat barrel cortex. *J Neurosci* 27:13316–13328.
30. Tsai PS, et al. (2009) Correlations of neuronal and microvascular densities in murine cortex revealed by direct counting and colocalization of nuclei and vessels. *J Neurosci* 29:14553–14570.
31. Nissl F (1894) Ueber eine neue Untersuchungsmethode des Centralorgans zur Feststellung der Localisation der Nervenzellen. *Neurologisches Centralblatt* 13:507–508.
32. Jones EG (1984) History of cortical cytology. *Cerebral Cortex: Cellular Components of the Cerebral Cortex*, eds Peters A, Jones EG (Plenum, New York), pp 1–28.
33. Lorente de Nó R (1949) Cerebral cortex: Architecture, intracortical connections, motor projections. *Physiology of the Nervous System*, ed Fulton JF (Oxford Univ Press, London), p 300.
34. Braak H (1984) Architectonics as seen by lipofuscin stains. *Cerebral Cortex: Cellular Components of the Cerebral Cortex*, eds Peters A, Jones EG (Plenum, New York), pp 59–99.
35. White EL, Keller A (1989) *Cortical Circuits: Synaptic Organization of the Cerebral Cortex: Structure, Function, and Theory* (Birkhauser, Boston).
36. Vogt C, Vogt O (1919) Allgemeinere Ergebnisse unserer Hirnforschung. *J Psychol Neurol* 25:273–462.
37. Lund JS (1973) Organization of neurons in the visual cortex, area 17, of the monkey (Macaca mulatta). *J Comp Neurol* 147:455–496.
38. Fitzpatrick D, Itoh K, Diamond IT (1983) The laminar organization of the lateral geniculate body and the striate cortex in the squirrel monkey (Saimiri sciureus). *J Neurosci* 3:673–702.
39. Lund JS, Wu CQ (1997) Local circuit neurons of macaque monkey striate cortex: IV. Neurons of laminae 1-3A. *J Comp Neurol* 384:109–126.
40. Somogyi P, Cowey A, Halász N, Freund TF (1981) Vertical organization of neurones accumulating 3H-GABA in visual cortex of rhesus monkey. *Nature* 294:761–763.
41. Hendry SH, Schwark HD, Jones EG, Yan J (1987) Numbers and proportions of GABA-immunoreactive neurons in different areas of monkey cerebral cortex. *J Neurosci* 7: 1503–1519.
42. Feldmeyer D, Lübke J, Silver RA, Sakmann B (2002) Synaptic connections between layer 4 spiny neurone-layer 2/3 pyramidal cell pairs in juvenile rat barrel cortex: Physiology and anatomy of interlaminar signalling within a cortical column. *J Physiol* 538:803–822.
43. Shepherd GM, Pologruto TA, Svoboda K (2003) Circuit analysis of experience-dependent plasticity in the developing rat barrel cortex. *Neuron* 38:277–289.
44. Petreanu L, Mao T, Sternson SM, Svoboda K (2009) The subcellular organization of neocortical excitatory connections. *Nature* 457:1142–1145.
45. Kerlin AM, Andermann ML, Berezovskii VK, Reid RC (2010) Broadly tuned response properties of diverse inhibitory neuron subtypes in mouse visual cortex. *Neuron* 67: 858–871.
46. Bureau I, von Saint Paul F, Svoboda K (2006) Interdigitated paralemniscal and lemniscal pathways in the mouse barrel cortex. *PLoS Biol* 4:e382.
47. Shepherd GM, Svoboda K (2005) Laminar and columnar organization of ascending excitatory projections to layer 2/3 pyramidal neurons in rat barrel cortex. *J Neurosci* 25:5670–5679.
48. Gur M, Snodderly DM (2008) Physiological differences between neurons in layer 2 and layer 3 of primary visual cortex (V1) of alert macaque monkeys. *J Physiol* 586: 2293–2306.
49. Lefort S, Tomm C, Floyd Sarria JC, Petersen CC (2009) The excitatory neuronal network of the C2 barrel column in mouse primary somatosensory cortex. *Neuron* 61:301–316.
50. Helmstaedter M, de Kock CP, Feldmeyer D, Bruno RM, Sakmann B (2007) Reconstruction of an average cortical column in silico. *Brain Res Brain Res Rev* 55:193–203.
51. Jones EG, Rakic P (2010) Radial columns in cortical architecture: It is the composition that counts. *Cereb Cortex* 20:2261–2264.
52. Helmstaedter M, Feldmeyer D (2010) Axons predict neuronal connectivity within and between cortical columns and serve as primary classifiers of interneurons in a cortical column. *New Aspects of Axonal Structure and Function*, eds Feldmeyer D, Lubke J (Springer, New York), pp 141–155.
53. Horton JC, Adams DL (2005) The cortical column: A structure without a function. *Philos Trans R Soc Lond B Biol Sci* 360:837–862.
54. da Costa NM, Martin KA (2010) Whose Cortical Column Would that Be? *Front Neuroanat* 4:16.
55. Gonchar Y, Wang Q, Burkhalter A (2007) Multiple distinct subtypes of GABAergic neurons in mouse visual cortex identified by triple immunostaining. *Front Neuroanat* 1:3.
56. Ascoli GA, et al.; Petilla Interneuron Nomenclature Group (2008) Petilla terminology: Nomenclature of features of GABAergic interneurons of the cerebral cortex. *Nat Rev Neurosci* 9:557–568.
57. Lee S, Hjerling-Leffler J, Zagha E, Fishell G, Rudy B (2010) The largest group of superficial neocortical GABAergic interneurons expresses ionotropic serotonin receptors. *J Neurosci* 30:16796–16808.
58. Lübke J, Roth A, Feldmeyer D, Sakmann B (2003) Morphometric analysis of the columnar innervation domain of neurons connecting layer 4 and layer 2/3 of juvenile rat barrel cortex. *Cereb Cortex* 13:1051–1063.
59. Helmstaedter M, Sakmann B, Feldmeyer D (2009) Neuronal correlates of local, lateral, and translaminar inhibition with reference to cortical columns. *Cereb Cortex* 19: 926–937.
60. Wong-Riley M (1979) Changes in the visual system of monocularly sutured or enucleated cats demonstrable with cytochrome oxidase histochemistry. *Brain Res* 171: 11–28.